Coupling of a high-energy excitation to superconducting quasiparticles in a cuprate from coherent charge fluctuation spectroscopy

Barbara Mansart[a,b], José Lorenzana[c], Andreas Mann[a], Ahmad Odeh[b], Mariateresa Scarongella[b], Majed Chergui[b], and Fabrizio Carbone[b,1]

[a]Laboratory for Ultrafast Microscopy and Electron Scattering, Institute of Condensed Matter Physics, and [b]Laboratory of Ultrafast Spectroscopy, Institute of Chemical Sciences and Engineering, Ecole Polytechnique Fédérale de Lausanne, CH-1015 Lausanne, Switzerland; and [c]Institute for Complex Systems–Consiglio Nazionale delle Ricerche, and Physics Department, University of Rome "La Sapienza," I-00185 Rome, Italy

Edited by Margaret M. Murnane, University of Colorado, Boulder, CO, and approved February 5, 2013 (received for review October 26, 2012)

Dynamical information on spin degrees of freedom of proteins or solids can be obtained by NMR and electron spin resonance. A technique with similar versatility for charge degrees of freedom and their ultrafast correlations could move the understanding of systems like unconventional superconductors forward. By perturbing the superconducting state in a high-T_c cuprate, using a femtosecond laser pulse, we generate coherent oscillations of the Cooper pair condensate that can be described by an NMR/electron spin resonance formalism. The oscillations are detected by transient broad-band reflectivity and are found to resonate at the typical scale of Mott physics (2.6 eV), suggesting the existence of a nonretarded contribution to the pairing interaction, as in unconventional (non-Migdal–Eliashberg) theories.

According to Bardeen–Cooper–Schrieffer (BCS) theory (1), superconductivity requires that electrons bind in Cooper pairs and condense collectively in a macroscopic quantum state. In conventional superconductors, the observation of a shift in the superconductivity transition temperature upon isotope substitution (2, 3) was an experimental breakthrough leading to the conclusion that lattice vibrations (phonons) act as a glue among electrons, promoting the required pairing. Since the discovery of high-temperature superconductivity in cuprates in 1986 (4), the observation of an analogous fingerprint of the glue involved in the pairing mechanism, if any, has been lacking.

A fertile route to obtain information on excitations in solids and their coupling to electrons is pump-probe spectroscopy (5). Typically, the sample is illuminated by an ultrashort laser pulse lasting a few tens of femtoseconds and carrying 1.5 eV photons. This "pump" pulse creates an out-of-equilibrium distribution of particle-hole excitations that decays to states within a few hundreds of millielectronvolts of the chemical potential (6) in the pulse duration timescale. There, phase space restrictions slow down the dynamics (7) and the subsequent evolution can be studied in real time by a probe pulse. The dynamical response of the system can be observed with a temporal resolution comparable to the timescale of relevant processes in the material, like the pairs breaking, their recombination, or the electron–phonon coupling time.

For example, the photoinduced quenching of the superconducting order parameter and its subsequent recovery were followed by recording the temporal evolution of the gap amplitude in the optical spectrum of different cuprates (8–11). Remarkably, it was found that the energy needed to suppress the superconducting state in these materials is several times larger than the condensation energy (9, 10), in contrast to what happens in conventional superconductors where it is of the same order (9, 11). Optical studies also provided insights on the relaxation dynamics of the excited quasiparticles (11–14) and on the optical spectral weight transfers associated with the carriers' kinetic energy changes across the photoinduced phase transition (15).

Femtosecond angle-resolved photoelectron spectroscopy (ARPES) showed that the decay of photoexcited carriers is dominated by the recombination of the Cooper pairs at the antinodes (i.e., the copper–oxygen bond direction in real space) (16). Also, similar experiments yielded an estimate of the electron–phonon coupling strength being in the intermediate regime (6), similar to what was found by femtosecond-electron diffraction, which in turns identified also its anisotropy (17, 18).

In all of the above-mentioned experiments, excitation by the pump occurs through dipole-allowed processes (i.e., the corresponding matter–radiation interaction Hamiltonian is linear as a function of the electric field) and the dynamics are dominated by the incoherent relaxation of the system. However, the same pump pulse can also generate coherent oscillations of the optical properties due to the population of elementary excitations through a stimulated Raman process (i.e., through the second-order term of the matter–radiation Hamiltonian, which is quadratic as a function of the electric field). For example, in transparent media, phonons can be excited by the impulsive stimulated Raman scattering (ISRS) mechanism (19, 20); in absorbing media instead, both a displacive (20–23) and an ISRS mechanism may enter into play, depending on various factors such as the lifetime of the particle-hole excitations (23)and the nature of the coupling among phonons and particle-hole excitations, etc.

In cuprates, the generation of coherent structural excitations (phonons) has already been reported (24, 25). More generally, any excitation that is active in spontaneous Raman scattering is also allowed in pump-probe spectroscopies. Indeed, Raman active electronic excitations like magnons and density fluctuations have been found to be coherently generated in different materials (26, 27).

In this report, we present a technique, coherent charge fluctuation spectroscopy (CCFS), in which charge fluctuations are coherently generated by the pump pulse through a stimulated Raman process active in a superconductor. These coherent excitations are subsequently probed by femtosecond-broad band reflectivity, allowing to observe the real-time oscillations of the Cooper pair condensate and its impact on high-energy excitations. CCFS takes advantage of the possibility to coherently control Cooper pairs in superconductors in a way that resembles the coherent control of spins with NMR-ESR techniques. To

Author contributions: F.C. designed research; B.M., J.L., A.M., A.O., M.S., M.C., and F.C. performed research; B.M., J.L., M.C., and F.C. analyzed data; and B.M., J.L., M.C., and F.C. wrote the paper.

The authors declare no conflict of interest.

This article is a PNAS Direct Submission.

Freely available online through the PNAS open access option.

[1]To whom correspondence should be addressed. E-mail: fabrizio.carbone@epfl.ch.

This article contains supporting information online at www.pnas.org/lookup/suppl/doi:10.1073/pnas.1218742110/-/DCSupplemental.

understand this analogy, it is useful to use Anderson's pseudospins formalism (28, 29).* The latter is based on the fact that despite their obvious physical difference, from a mathematical (or purely formal) point of view, magnetism and superconductivity are closely linked phenomena.

The BCS wave function of a generic superconductor reads

$$|\Psi\rangle = \prod_k \left(u_{\mathbf{k}} + v_{\mathbf{k}} c^{\dagger}_{\mathbf{k}\uparrow} c^{\dagger}_{-\mathbf{k}\downarrow}\right)|0\rangle, \qquad [1]$$

where the operator $c^{\dagger}_{\mathbf{k}\sigma}$ creates an electron with spin σ and wavevector $\mathbf{k}$ and $|0\rangle$ represents the vacuum state. For each pair of states $(\mathbf{k}\uparrow, -\mathbf{k}\downarrow)$ the wave function is a quantum mixture of the pair being empty (with amplitude u_k) and being fully occupied (with amplitude v_k). Anderson's idea is illustrated pictorially in Fig. 1 and consists of representing the fully occupied pair $(\mathbf{k}\uparrow, -\mathbf{k}\downarrow)$ by a down pseudospin in momentum space (Fig. 1*A*) and the state in which the pair is empty by an up pseudospin (Fig. 1*B*).* The advantage of this representation is that the pseudospins behave like traditional spin-1/2 operators, and the quantum mixture of fully occupied and empty states in the BCS wave function is represented by a sidewise pseudospin (Fig. 1*C*).

In the normal state $u_k = 0$ and v_k is different from zero only for states inside the Fermi surface, which corresponds to empty pairs above the chemical potential (up pseudospins) and fully occupied pairs below the chemical potential (down pseudospins), leading to the pseudospin texture shown schematically in Fig. 1*D*, with a sharp interface at the Fermi surface. In the superconducting state, mixing of empty and fully occupied pairs, which becomes maximum at the chemical potential, blurs the Fermi surface, leading to the texture shown in Fig. 1*E*.

Coherent control of the pseudospins in a superconductor can be achieved by an ad hoc prepared light pulse through a stimulated Raman process that, as discussed in more detail below, triggers the precession of the pseudospins around their equilibrium axis. This is analogous to NMR and ESR experiments in which magnetic field pulses induce a precession of real spins (30). The concept and schematics of this experiment are depicted in Fig. 1 *F* and *G*. An infrared polarized femtosecond laser pulse couples to charge fluctuations in a superconductor according to Raman selection rules. The pump pulse impulsively perturbs the system and induces the pseudospins' precession, i.e., the oscillations of the Cooper pair condensate. The optical spectra of the system are then monitored in real time at different energies, revealing the optical transitions that respond to the oscillating condensate; this allows us to single out those excitations that can potentially mediate electron–electron interactions impacting the formation of Cooper pairs. This is of pivotal importance for cuprates, because the applicability of conventional pairing theories (31), based on retarded interactions between electrons mediated by low-energy glue bosons, has been doubted (32, 33) and a completely different framework has been proposed involving nonretarded interactions associated with electronic high-energy scales (34).

We performed such high-temporal-resolution (<50 fs) experiments in two optimally doped ($T_c = 40$ K) $La_{2-x}Sr_xCuO_4$ (LSCO) single crystals ($x = 0.15$) with different orientations (see *SI Text* and ref. 35 for details). A polarized 1.55-eV laser pulse with a duration of 45 fs and an absorbed fluence around 300 μJ/cm^2 (unless otherwise stated) induces both dipole (linear in the electric field) and Raman (quadratic in the electric field) allowed excitations, the latter being the main focus of this work.

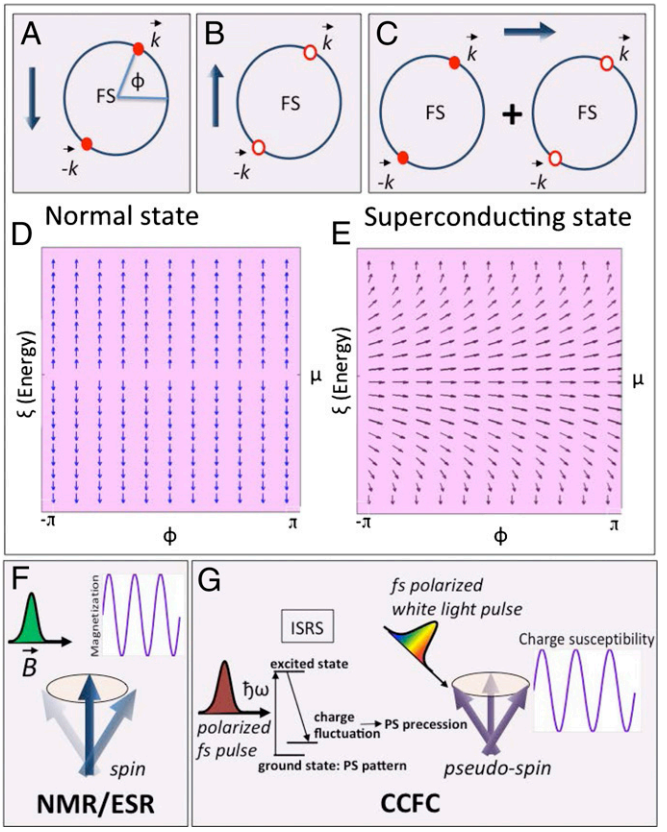

Fig. 1. Pseudospin description of the coherent charge fluctuation spectroscopy experiment. (*A*) Angle ϕ along the Fermi surface (FS). *A–C* define the pseudospin operators in momentum space: A pseudopsin down corresponds to the pair of states $(\mathbf{k}\uparrow, -\mathbf{k}\downarrow)$ being fully occupied (*A*), a pseudospin up to the pair $(\mathbf{k}\uparrow, -\mathbf{k}\downarrow)$ being empty (*B*), and a sideways pseudopsin to a quantum superposition of the previous two (*C*). (*D* and *E*) Pseudospin pattern in the normal state and in the case of an *s*-wave superconductor, respectively. Rather than plotting the pseudospins as a function of momentum $\mathbf{k}$ we make a change of coordinates and plot as a function of the Fermi surface angle ϕ and the energy distance ξ of the state $\mathbf{k}$ from the chemical potential μ. (*F*) Schematic view of an NMR/ESR experiment in which the spins precess, inducing a magnetization oscillation. (*G*) Corresponding view for a CCFS experiment, in which the pseudospins precess upon ultrafast excitation and coherent charge fluctuation generation.

We chose different experimental geometries for exploiting the Raman selection rules for excitation and detection to obtain information on different final states (*SI Text*). In the first geometry, the pump electric field is parallel to the Cu-O bond, giving access to Raman excitations with $A_{1g} + B_{1g}$ symmetry, whereas the probe-pulse electric field is directed toward the *c* axis, allowing us to detect only A_{1g} symmetry excitations. Then, using the same pumping geometry, we probed the excited system along [100] and [010], which respectively give access to $A_{1g} + B_{1g}$ and $A_{1g} - B_{1g}$ excitations. Performing the difference between the two orientations allows us to extract only B_{1g} excitations. Finally, we used the pumping and probing fields on the diagonal direction giving access to $A_{1g} + B_{2g}$ Raman excitations. The dynamics of all these excitations are then probed by broad-band ultrafast reflectivity, for which overall time-energy dependence is displayed in Fig. 2 *A–C*.

The transient reflectivity is dominated by a large abrupt amplitude change followed by a relaxation; this is a consequence of high-energy particle-hole (*p-h*) excitations produced by the dipole allowed absorption of the pump photons. Furthermore, in both orientations the transient reflectivity changes sign throughout the

*The pseudospin operators are defined as $\sigma^x_k = (c_{k\uparrow}c_{-k\downarrow} + h.c.)$, $i\sigma^y_k = (c_{k\uparrow}c_{-k\downarrow} - h.c.)$, and $\sigma^z_k = 1 - n_{k\uparrow} - n_{-k\downarrow}$. Here $n_{k\sigma} = c^{\dagger}_{k\sigma}c_{k\sigma}$ and $c^{\dagger}_{k\sigma}$ ($c_{k\sigma}$) are creation (annihilation) operators for electrons.

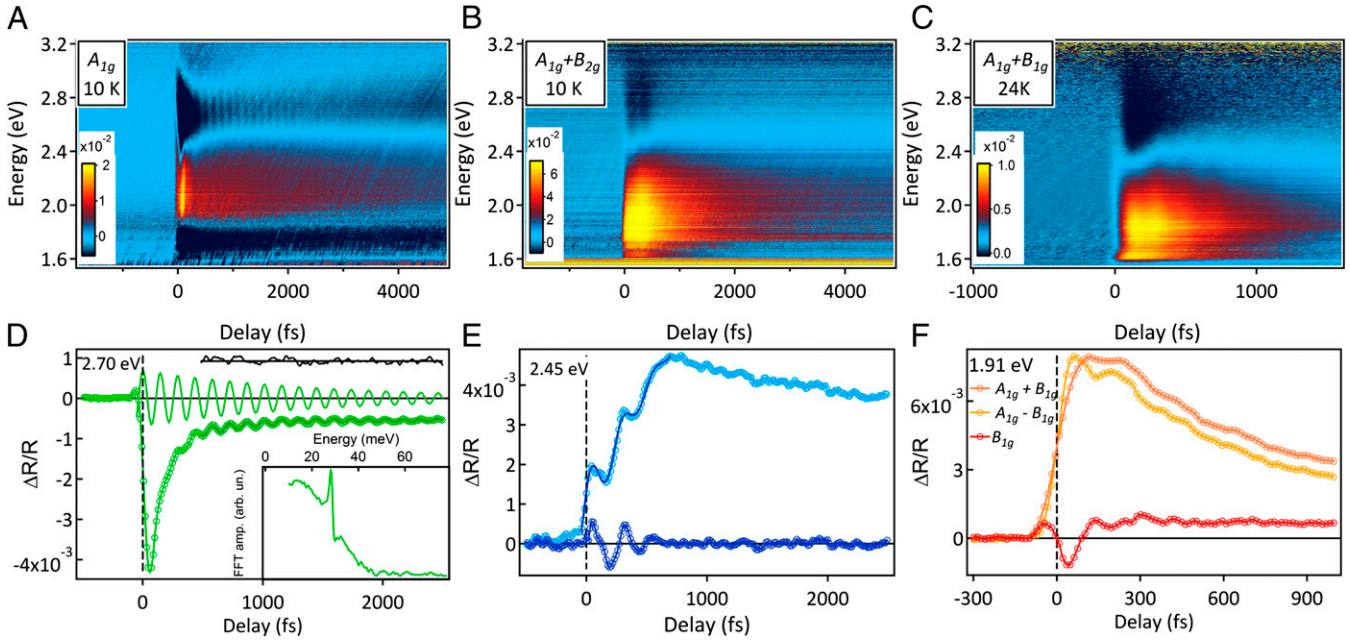

Fig. 2. (*A–F*) Transient broad-band reflectivity data at 10 K in A_{1g} {pump ∥ [100], probe ∥ [001], (*A* and *D*)} and $A_{1g} + B_{2g}$ {pump ∥ [110], probe ∥[110], (*B* and *E*)} and at 24 K in $A_{1g} + B_{1g}$ {pump ∥ [100], probe ∥ [100], (*C* and *F*)} geometries (specified in tetragonal axis). The extracted profiles are shown in *C* and *F* for selected probe energies. *E* presents the reflectivity oscillations by substracting the background on the profile, and in *F* we show the difference between $A_{1g} + B_{1g}$ and $A_{1g} - B_{1g}$ profiles, which is proportional to the B_{1g} signal. The absorbed pump fluence is around 300 μJ/cm^2.

spectra in correspondence to specific electronic transitions. These changes reflect the transfer of spectral weight among the different absorption bands produced by the *p-h* excitations (15). The number of *p-h* excitations involved is estimated in *SI Text* to be less than 10^{-2} per Cu atom.

All geometries present coherent oscillations of Raman excitations on top of the dipole *p-h* excitations relaxation as shown in the temporal profiles in Fig. 2 *D–F*, taken at selected energies where the oscillation amplitude is the largest. These profiles are representative of the full datasets for a given geometry as far as the oscillation phase and frequency are concerned. In A_{1g} symmetry, an ultrafast oscillation with a period of 145 fs and a long coherence time (1.45 ps) is visible at all wavelengths (Fig. 2 *A* and *D*). The Fourier transform analysis of A_{1g} symmetry data is presented in Fig. 2*D*, *Inset*. A sharp peak at 28 meV is visible, corresponding to the out-of-plane La A_{1g} mode of LSCO (36); the corresponding atomic motions are shown in Movie S1. Such coherent fully symmetric modes have already been observed in high-T_c superconductors (22, 24).

Instead, in both $A_{1g} + B_{2g}$ and B_{1g} symmetries (Fig. 2 *E* and difference in *F*), slower and damped (around 300 fs coherence time) oscillations are clearly observed below T_c. The Fourier analysis of these time-resolved profiles is presented in Fig. 3 *A* and *B*. In $A_{1g} + B_{2g}$ symmetry, for a probing wavelength of 2.45 eV, the temperature dependence of the Fourier-transform signal shows an obvious peak at 18 meV that vanishes above T_c (Fig. 3*B*). In B_{1g} symmetry, the broad peak appears at energies around 24 meV when the sample temperature is lower than T_c. Increasing the pump fluence to 2 mJ/cm^2, no such peak could be observed below T_c (Fig. 3*A*).

In Fig. 3 *C* and *D* we display the terahertz spectra obtained in the superconducting state and compare them with the spontaneous Raman response (data taken from ref. 36), which is well understood in terms of the excitation of two Bogoliubov quasiparticles (37). The good agreement between them allows us to identify the strongly temperature-dependent part of the oscillations as Raman charge fluctuations of the superconducting condensate. This agreement is expected from simple theoretical considerations for electronic ISRS, which show that any excitation that is Raman active in a colinear configuration of incoming and outgoing photon electric fields is also accessible in a pump-probe experiment (*SI Text*). Our experiment detects remnants of superconductivity at fluences of the same order but larger than previously reported (10, 16). We attribute that difference to the much higher sensitivity of our optical measurement to superconductivity and its bulk character. Presumably, superconductivity is indeed quenched on the first layers of the sample and becomes invisible to surface probes like photoelectron spectroscopies (16).

The temporal evolution of the coherent phonon oscillation in A_{1g} geometry is presented in Fig. 2*D*, with its extrapolation down to zero-time delay (as defined in ref. 35), allowing us to establish its cosine waveform that is typical of a displacive (resonant) mechanism of excitation (20, 21). The electronic transitions induced by 1.55-eV photons occur between the ground state of the material and higher-energy electronic states. At this energy, a peak in the optical absorption is observed in LSCO, distinct from the Cu-O charge transfer (38), which had been attributed to charge ordering in the form of stripes (39). Thus, the cosine wave form indicates that, not unexpectedly, the charge modulations are strongly coupled to the A_{1g} La phonon.

In the A_{1g} geometry, the presence of the strong coherent phonon disturbs the real-time observation of the superconducting condensate. Instead, in both $A_{1g} + B_{2g}$ and B_{1g} symmetries, the fluctuations of the superconducting quasiparticles are clearly observable and start at zero time delay, allowing the determination of a sine waveform (Fig. 2 *E* and *F*). This indicates that contrary to the A_{1g} phonon case, the triggering mechanism is ISRS (19, 20), meaning that the *p-h* excitations at the energy of the pump pulse are not directly coupled to the superconducting quasiparticles. We show below that an analysis of the probe energy dependence leads to the same conclusion.

For the Raman allowed excitations, the effect of the pump light on the electrons can be described by a time-dependent impulsive

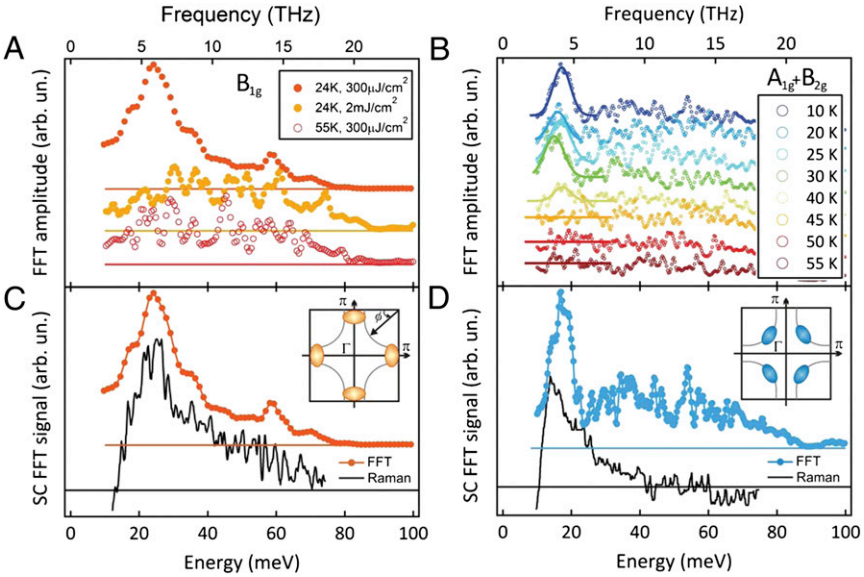

Fig. 3. (*A* and *B*) Fourier transform spectra obtained at different temperatures and excitation fluences in B_{1g} (*A*, 1.91 eV probing energy) and $A_{1g} + B_{2g}$ (*B*, 2.45 eV probing energy) geometries. (*C* and *D*) Comparison between transient reflectivity data and Raman measurements, in the superconducting phase. The spontaneous Raman spectra are the difference between superconducting and normal phases, showing only the charge fluctuation peaks. *Insets* show schematically in *C* the angle ϕ along the Fermi surface and the regions in momentum space excited in B_{1g} symmetry and in *D* the same for B_{2g} symmetry.

potential quadratic in the electric field (*SI Text*).[†] As mentioned above, we can describe its effect on the superconducting quasiparticles using Anderson's pseudospin formalism (28).

The reduced BCS Hamiltonian in the presence of a time-dependent potential acquires a simple form when written in terms of the pseudospin operators $\boldsymbol{\sigma}_{\mathbf{k}}$,*

$$H = -\sum_{\mathbf{k}} \mathbf{b}_{\mathbf{k}}.\boldsymbol{\sigma}_{\mathbf{k}}, \qquad [2]$$

where $\boldsymbol{\sigma}_{\mathbf{k}}$ is a Pauli matrix representing the pseudospin associated with the pair of states $(\mathbf{k}\uparrow, -\mathbf{k}\downarrow)$ and $\mathbf{b}_{\mathbf{k}}$ is a fictitious "magnetic field". At the equilibrium, pseudospins orient parallel to the ground-state pseudomagnetic field $\mathbf{b}^0_{\mathbf{k}} = (\Delta_{\mathbf{k}}, 0, \xi_{\mathbf{k}})$, where $\Delta_{\mathbf{k}}$ is the superconducting order parameter and $\xi_{\mathbf{k}} = \epsilon_{\mathbf{k}} - \mu$, $\epsilon_{\mathbf{k}}$ being the quasiparticle band energy (in the absence of superconductivity) and μ the chemical potential. Thus, this Hamiltonian expresses the familiar fact that the ground-state wave function is determined by the mean-field order parameter $\Delta_{\mathbf{k}}$, which in turn can be expressed in terms of the pseudospins.

In the absence of superconductivity, $\Delta_{\mathbf{k}} = 0$; so the pseudomagnetic field points in the z direction and changes sign at the chemical potential, leading to the equilibrium texture of Fig. 1*D*. In the superconducting state, the pseudomagnetic field acquires a horizontal component, $\Delta_{\mathbf{k}} \neq 0$, so that in the case of an *s*-wave superconductor the pseudospins display the texture shown in Fig. 1*E*. For a *d*-wave superconductor, the horizontal component of the pseudomagnetic field cancels along the nodal directions due to the gap anisotropy, leading to the texture of Fig. 4*A*, which has no sideway pseudospins along the nodal direction.

The Raman coupling to the pump pulse can be described by a time-dependent potential $v^X_{\mathbf{k}}(t)$ coupling to charge fluctuations, i.e., to the z component of the pseudospins. The potential has a different dependence in momentum space depending on the symmetry $X = A_{1g}, B_{1g}, B_{2g}$, which is determined by the polarization of the pump (*SI Text*).*,[†] Thus, the pseudomagnetic field becomes time dependent: $\mathbf{b}_{\mathbf{k}}(t) = \mathbf{b}^0_{\mathbf{k}} + \delta\mathbf{b}_{\mathbf{k}}(t)$, with $\delta\mathbf{b}_{\mathbf{k}}(t) = \left(0, 0, v^X_{\mathbf{k}}(t)\right)$. The pseudospins obey the usual equations of motion for magnetic moments in a time-dependent magnetic field (28),

$$\hbar \frac{\partial \boldsymbol{\sigma}_{\mathbf{k}}}{\partial t} = -2[\mathbf{b}^0_{\mathbf{k}} + \delta\mathbf{b}_{\mathbf{k}}(t)] \times \boldsymbol{\sigma}_{\mathbf{k}}, \qquad [3]$$

implying that after the pulse passage the pseudospins precess around the equilibrium direction with an angular velocity $2|\mathbf{b}^0_{\mathbf{k}}|/\hbar$, with $|\mathbf{b}^0_{\mathbf{k}}| = \sqrt{\xi^2_{\mathbf{k}} + \Delta^2_{\mathbf{k}}}$ being the BCS quasiparticle energy (Fig. 4*B*, Fig. S1, and Movie S2).

Eq. **3** is close to the equation of motion used in NMR/ESR formalisms; however, in NMR the static field $\mathbf{b}^0$ is usually provided by an external field, whereas here it is due to the interaction with the other pseudospins. The magnetic analogy is actually more complete with ESR in magnetically ordered materials where $\mathbf{b}^0$ can be completely due to the interaction with the other spins.

Because $\delta\mathbf{b}_{\mathbf{k}}$ is in the z direction, only pseudospins having a significant component at equilibrium in the x-y plane respond to the Raman impulsive field, automatically selecting the quasiparticles participating in the pairing. This is further constrained by the momentum-dependent form factors in $v^X_{\mathbf{k}}(t)$.[†] Therefore, in B_{2g} symmetry only pseudospins that are close to the Fermi level and are neither in the nodes nor in the antinodes have a significant time dependence. The oscillating z projection of the pseudospins shown in Fig. 4*B* encodes the contribution to the total charge fluctuation, shown in Fig. 4*C*. At $t = 50$ fs (blue) the pseudospins at $\xi = 0$ and close to $\phi = \pi/4 \pm \pi/8$ are close to their maximum negative amplitude in the z direction, corresponding to the first peak in the B_{2g} charge fluctuation.

We also show in Fig. 4*C* a comparison between the experimental and theoretical condensate oscillation in B_{2g} geometry. Interestingly, the experiment shows a quite long coherence time compared with theory. Details of the computations are given in *SI Text*.

[†] Charge fluctuations are defined by the operator $N_X = \sum_{k\sigma} f^X_k n_{k\sigma}$, with $f^{B_{1g}}_k = [\cos(k_x a) - \cos(k_y a)]/2$, and $f^{B_{2g}}_k = \sin(k_x a)\sin(k_y a)$. The Raman time-dependent potentials produced by the pump electric field, E, are $v^X_k(t) = f^X_k v_X(t)$ with $v_X(t) = -\frac{1}{2}E(t).\partial\chi(\omega_L)/\partial\langle N_X\rangle.E(t)$ with χ the charge susceptibility and its density derivative the conventional Raman tensor (*SI Text*).

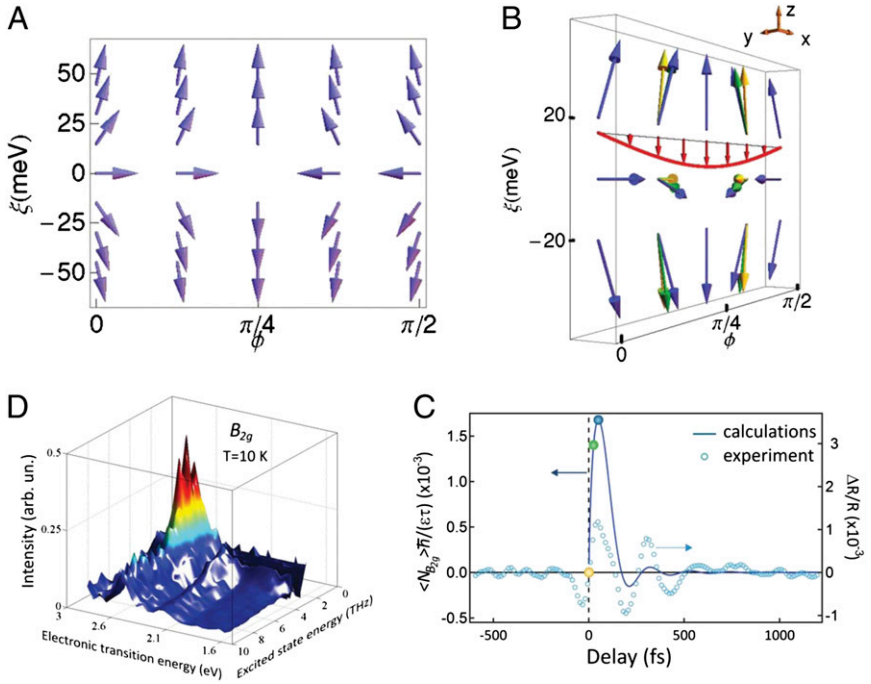

Fig. 4. Pseudospin textures coding the BCS wave function in momentum space. (*A*) Ground state texture: Pseudospins are labeled by the distance in energy from the Fermi level $\xi \equiv \xi_k$ and the angle ϕ along the Fermi surface (Fig. 2*C*, *Inset*). (*B*, short red arrows) Amplitude of the impulsive field $\delta \mathbf{b}_k$ applied at $t = 0$ in B_{2g} symmetry. (Long arrows) Texture snapshots (amplitudes exaggerated for clarity) immediately after the excitation (yellow), at 25 fs (green), and at 50 fs (blue). (*C*) Theoretical charge fluctuation: Solid circles correspond to the snapshots in *B*. Open circles represent the experimental change in reflectivity after the high-energy $p - h$ background has been subtracted. (*D*) Probe energy dependence of the Fourier-transformed $A_{1g} + B_{2g}$ fluctuation.

The transient optical properties of the system in the presence of a fluctuation of symmetry X are governed by the changes in the dielectric function tensor

$$\delta\boldsymbol{\varepsilon}(\omega, t) = -4\pi \sum_X \frac{\partial \boldsymbol{\chi}}{\partial \langle N_X \rangle}(\omega) \langle N_X \rangle(t), \qquad [4]$$

and $\partial\boldsymbol{\chi}/\partial\langle N_X\rangle$ is the conventional Raman tensor (*SI Text*). We see that the same Raman tensor appears in the generation of the pulse by ISRS and in the subsequent probing process. In analogy with lattice ISRS (20), only excitations having an interaction matrix element with the fluctuating quasiparticles will contribute to $\partial\boldsymbol{\chi}/\langle N_X\rangle$, allowing us to detect excitations participating in the pairing. We point out that CCFS is not restricted to reflectivity, and other techniques like spontaneous Raman scattering can be used as a probe, allowing us to test also excitations of different symmetries. In this case a different matrix element will be involved in the probe in lieu of the Raman tensor in Eq. **4**.

The oscillation of the superconducting condensate is most clearly visible in the $A_{1g} + B_{2g}$ configuration. For this reason, we perform the spectral analysis in this configuration. The probe-energy dependence of the $A_{1g} + B_{2g}$ fluctuation in the frequency domain is presented in Fig. 4*D*. The superconducting fluctuations clearly resonate at an energy of 2.6 eV, corresponding to the Cu-O charge transfer energy of the parent compound that coincides with the Hubbard energy U of a one-band description (32). Remarkably, even though there is substantial absorption below the charge transfer band in our samples, the superconducting quasiparticles appear to be decoupled from the excitations in that energy region. This is fully consistent with our finding above that the $A_{1g} + B_{2g}$ fluctuations have a sine waveform when pumped at 1.55 eV.

The correct framework to understand superconductivity in cuprates has been the subject of an intense debate (32, 33, 40). One possibility is that the role of phonons in the traditional mechanism is replaced by a different low-energy bosonic excitation like damped magnons, which act as a glue, allowing the pairing of electrons (41, 42). In this scenario, superconductivity can be understood in the traditional framework (31) where retardation plays an important role. Anderson (32) has argued that there is no such low-energy glue and that proximity to the Mott phase is an essential ingredient. The relevant timescale of the interactions inducing the pairing is the inverse of the Hubbard energy $U \gtrsim 2$ eV. Therefore, the interaction can be considered instantaneous for practical purposes. Our results are consistent with a coupling of the superconducting quasiparticles with excitations at 2.6 eV. We attribute this to a fingerprint of "Mottness" in the superconducting state, although we cannot exclude other electronic transitions like a $d - d$ exciton, which would also be interesting. Systematic studies of these types of oscillations in different chemical compositions and energy ranges coupled to further theoretical work may allow us to gain deeper insights into the pair-mediating or pair-breaking nature of these excitations.

A negligible coupling in the rest of the measured energy window (1.6 eV $< \hbar\omega <$ 3.2 eV) is observed, but we cannot exclude that other electronic excitations outside our probing range are also coupled to superconductivity and even dominant. Numerical computations support a coupling to the Mott scale (40), although with a strong contribution from the low-energy region.

The key feature of the isotope effect (2, 3) in conventional superconductors was its high specificity, because only the frequency of one potential glue excitation was affected and its impact on superconductivity evaluated. CCFS has a high degree of specificity in a reverse form: Only paired electrons are affected, and their impact on different excitations is assessed.

Compared with previous ultrafast studies of superconductivity, our experiments provide a direct observable of the coherent Cooper pairs dynamics. Moreover, because of the spectroscopic nature of our probing scheme, we can detect resonances between superconductivity and high-energy excitations. Also, because we

directly obtain the condensate oscillations in real time, we have access to their phase and its evolution throughout the probing energy range. The presented results form a benchmark for time-resolved experiments in cuprates and shed new light on the nature of the pairing interactions.

In a more general perspective the NMR/ESR analogy encoded in Eqs. **2** and **3** allows us to borrow concepts like the relaxation times T_1 and T_2^* (30). T_2^* is defined by the decay of the charge fluctuations, which is dominated by the inhomogeneity of the pseudomagnetic field in momentum space. Therefore, our experiment opens appealing perspectives to typical NMR/ESR-like techniques such as coherent control of the superconducting wave function by a sequence of pulses. These tools can be generally applied to different materials, including heavy fermions and iron-based superconductors.

ACKNOWLEDGMENTS. The authors acknowledge useful discussions with A. B. Kuzmenko and D. Fausti. This work was supported by the Swiss National Science Foundation via the Contracts *PP*00*P*2–128269 and 20020–127231/1. J.L. is supported by Italian Institute of Technology–Seed Project NEWDFESCM (New Density Functionals for the Electronic Structure of Correlated Materials).

1. Bardeen J, Cooper LN, Schrieffer JR (1957) Theory of superconductivity. *Phys Rev* 108: 1175–1204.
2. Maxwell E (1950) Isotope effect in the superconductivity of mercury. *Phys Rev* 78(4):477.
3. Reynolds CA, Serin B, Wright WH, Nesbitt LB (1950) Superconductivity of isotopes of mercury. *Phys Rev* 78(4):487.
4. Bednorz JG, Müller KA (1986) Possible high-T_c superconductivity in the Ba-La-Cu-O system. *Z Phys B* 64:189–193.
5. Orenstein J (2012) Ultrafast spectroscopy of quantum materials. *Phys Today* 65:44.
6. Perfetti L, et al. (2007) Ultrafast electron relaxation in superconducting $Bi_{(2)}Sr_{(2)}CaCu_{(2)}O_{(8+\delta)}$ by time-resolved photoelectron spectroscopy. *Phys Rev Lett* 99(19):197001.
7. Howell PC, Rosch A, Hirschfeld PJ (2004) Relaxation of hot quasiparticles in a *d*-wave superconductor. *Phys Rev Lett* 92(3):037003.
8. Kaindl RA, et al. (2000) Ultrafast mid-infrared response of YBa(2)Cu(3)O(7-δ). *Science* 287(5452):470–473.
9. Stojchevska L, et al. (2011) Mechanisms of nonthermal destruction of the superconducting state and melting of the charge-density-wave state by femtosecond laser pulses. *Phys Rev B* 84:180507.
10. Pashkin A, et al. (2010) Femtosecond response of quasiparticles and phonons in superconducting $YBa_{(2)}Cu_{(3)}O_{(7-\delta)}$ studied by wideband terahertz spectroscopy. *Phys Rev Lett* 105(6):067001.
11. Beck M, et al. (2011) Energy-gap dynamics of superconducting NbN thin films studied by time-resolved terahertz spectroscopy. *Phys Rev Lett* 107(17):177007.
12. Gedik N, et al. (2004) Single-quasiparticle stability and quasiparticle-pair decay in $YBa_2Cu_3O_{6.5}$. *Phys Rev B* 70:014504.
13. Gedik N, et al. (2005) Abrupt transition in quasiparticle dynamics at optimal doping in a cuprate superconductor system. *Phys Rev Lett* 95(11):117005.
14. Kabanov VV, Demsar J, Mihailovic D (2005) Kinetics of a superconductor excited with a femtosecond optical pulse. *Phys Rev Lett* 95(14):147002.
15. Giannetti C, et al. (2011) Revealing the high-energy electronic excitations underlying the onset of high-temperature superconductivity in cuprates. *Nat Commun* 2:353.
16. Cortés R, et al. (2011) Momentum-resolved ultrafast electron dynamics in superconducting $Bi_2Sr_2CaCu_2O(8+\delta)$. *Phys Rev Lett* 107(9):097002.
17. Carbone F, Yang DS, Giannini E, Zewail AH (2008) Direct role of structural dynamics in electron-lattice coupling of superconducting cuprates. *Proc Natl Acad Sci USA* 105(51): 20161–20166.
18. Carbone F, Gedik N, Lorenzana J, Zewail AH (2010) Real-time observation of cuprates structural dynamics by ultrafast electron crystallography. *Adv Condens Matter Phys* 2010:958618.
19. Merlin R (1997) Generating coherent *THz* phonons with light pulses. *Solid State Commun* 102:207–220.
20. Stevens TE, Kuhl J, Merlin R (2002) Coherent phonon generation and the two stimulated Raman tensors. *Phys Rev B* 65:144304.
21. Zeiger HJ, et al. (1992) Theory for displacive excitation of coherent phonons. *Phys Rev B* 45(2):768–778.
22. Mazin II II, Liechtenstein AI, Jepsen O, Andersen OK, Rodriguez CO (1994) Displacive excitation of coherent phonons in $YBa_2Cu_3O_7$. *Phys Rev B* 49(13):9210–9213.
23. Riffe DM, Sabbah AJ (2007) Coherent excitation of the optic phonon in Si: Transiently stimulated Raman scattering with a finite-lifetime electronic excitation. *Phys Rev B* 76:085207.
24. Albrecht W, Kruse Th, Kurz H (1992) Time-resolved observation of coherent phonons in superconducting $YBa_2Cu_3O_{7-\delta}$ thin films. *Phys Rev Lett* 69(9):1451–1454.
25. Misochko OV, Georgiev N, Dekorsy T, Helm M (2002) Two crossovers in the Pseudogap regime of $YBa_2Cu_3O_{(7-\delta)}$ superconductors observed by ultrafast spectroscopy. *Phys Rev Lett* 89(6):067002.
26. Zhao J, Bragas AV, Lockwood DJ, Merlin R (2004) Magnon squeezing in an antiferromagnet: Reducing the spin noise below the standard quantum limit. *Phys Rev Lett* 93(10):107203.
27. Bao JM, Pfeiffer LN, West KW, Merlin R (2004) Ultrafast dynamic control of spin and charge density oscillations in a GaAs quantum well. *Phys Rev Lett* 92(23):236601.
28. Anderson PW (1958) Random-phase approximation in the theory of superconductivity. *Phys Rev* 112:1900–1916.
29. Warner GL, Leggett AJ (2005) Quench dynamics of a superfluid Fermi gas. *Phys Rev B* 71:134514.
30. Slichter CP (1996) *Principles of Magnetic Resonance,* Springer Series in Solid-State Sciences (Springer, Berlin), Vol 1.
31. Eliashberg GM (1960) Interactions between electrons and lattice vibrations in a superconductor. *Sov Phys JETP* 11:696–702.
32. Anderson PW (2007) Physics. Is there glue in cuprate superconductors? *Science* 316(5832):1705–1707.
33. Zaanen J (2011) *A Modern, but Way Too Short History of the Theory of Superconductivity at a High Temperature, in 100 Years of Superconductivity*, eds Rogalla H, Kes PH (Taylor & Francis, New York).
34. Anderson PW (1987) The resonating valence bond state in La_2CuO_4 and superconductivity. *Science* 235(4793):1196–1198.
35. Mansart B, et al. (2012) Evidence for a Peierls phase-transition in a three-dimensional multiple charge-density waves solid. *Proc Natl Acad Sci USA* 109(15):5603–5608.
36. Sugai S, Suzuki H, Takayanagi Y, Hosokawa T, Hayamizu N (2003) Carrier-density-dependent momentum shift of the coherent peak and the LO phonon mode in *p*-type high-T_c superconductors. *Phys Rev B* 68:184504.
37. Devereaux TP, Hackl R (2007) Inelastic light scattering from correlated electrons. *Rev Mod Phys* 78:175–233.
38. Uchida S, et al. (1991) Optical spectra of $La_{2-x}Sr_xCuO_4$: Effect of carrier doping on the electronic structure of the CuO_2 plane. *Phys Rev B* 43(10):7942–7954.
39. Lorenzana J, Seibold G (2003) Dynamics of metallic stripes in cuprates. *Phys Rev Lett* 90(6):066404.
40. Maier TA, Poilblanc D, Scalapino DJ (2008) Dynamics of the pairing interaction in the hubbard and t-J models of high-temperature superconductors.. *Phys Rev Lett* 100(23): 237001.
41. Scalapino DJ (1995) The case for $d_{x^2-y^2}$ pairing in the cuprate superconductors. *Phys Rep* 250:329–365.
42. Pines D (1997) Nearly antiferromagnetic Fermi liquids: A progress report. *Zeitschrift für Physik B* 103:129–135.